AAPS PharmSciTech 2007; 8 (4) Article 99 (http://www.aapspharmscitech.org).

Raman Characterization and Chemical Imaging of Biocolloidal Self-Assemblies, Drug Delivery Systems, and Pulmonary Inhalation Aerosols: A Review

Received: November 30, 2006; Final Revision Received: June 9, 2007; Accepted: June 11, 2007; Published: November 30, 2007

Heidi M. Mansour[1] and Anthony J. Hickey[1]

[1]University of North Carolina at Chapel Hill, School of Pharmacy, Division of Molecular Pharmaceutics, Campus Box #7360, 1311 Kerr Hall, Dispersed Systems Laboratory, Chapel Hill, NC 27599-7360

ABSTRACT

This review presents an introduction to Raman scattering and describes the various Raman spectroscopy, Raman microscopy, and chemical imaging techniques that have demonstrated utility in biocolloidal self-assemblies, pharmaceutical drug delivery systems, and pulmonary research applications. Recent Raman applications to pharmaceutical aerosols in the context of pulmonary inhalation aerosol delivery are discussed. The "molecular fingerprint" insight that Raman applications provide includes molecular structure, drug-carrier/excipient interactions, intramolecular and intermolecular bonding, surface structure, surface and interfacial interactions, and the functional groups involved therein. The molecular, surface, and interfacial properties that Raman characterization can provide are particularly important in respirable pharmaceutical powders, as these particles possess a higher surface-area-to-volume ratio; hence, understanding the nature of these solid surfaces can enable their manipulation and tailoring for functionality at the nanometer level for targeted pulmonary delivery and deposition. Moreover, Raman mapping of aerosols at the micro- and nanometer level of resolution is achievable with new, sophisticated, commercially available Raman microspectroscopy techniques. This noninvasive, highly versatile analytical and imaging technique exhibits vast potential for in vitro and in vivo molecular investigations of pulmonary aerosol delivery, lung deposition, and pulmonary cellular drug uptake and disposition in unfixed living pulmonary cells.

KEYWORDS: Spectroscopy, microscopy, imaging, molecular, interfacial, lung, mapping.

Corresponding Author: Heidi M. Mansour, University of North Carolina at Chapel Hill, School of Pharmacy, Division of Molecular Pharmaceutics, Campus Box #7360, 311 Pharmacy Lane, 1311 Kerr Hall, Dispersed Systems Laboratory, Chapel Hill, NC 27599-7360. Tel: (919) 966-0484; Fax: (919) 966-0197; E-mail: hmmansour@unc.edu

INTRODUCTION—THE RAMAN EFFECT

Elastic scattering of photons (Rayleigh scattering) from incoming light occurs with the same frequency (energy) and hence wavelength as the incident photons, as depicted in Figure 1a. The Raman effect was discovered by the Indian physicist Sir Chandrasekhara Venkata Raman, who was awarded the Nobel Prize in Physics in 1930 for his seminal discoveries on the "molecular diffraction of light" in liquids and the "diffusion of gases."[1-3] The Raman effect is the process whereby inelastic scatter of outgoing photons occurs, which is typically a small fraction of scattered photons at a different and higher optical frequency from the incident photonic frequency. Raman shift in wave numbers (cm^{-1}) is defined as the difference between the incident light, $\lambda_{incident}$, and the Raman scattering of photons, $\lambda_{scattered}$. In other words, the vibrational energy of the scattering molecule is the energy difference between the incident and Raman-scattered photons. A typical Raman spectrum consists of a plot of the scattered light as a function of the energy difference. Figure 1 illustrates the scattering effects that give rise to the Raman effect, which occurs when the incident photon interacts with the electric dipole of the molecule, pertubating the molecule's electrical field. This is a quantum mechanical phenomenon, whereby the scattering can be described as a vibrational energy change resulting from an excitation to a lower energy state rather than a real electronic transition. The scattered photon will have a longer wavelength (lower energy) than the incoming photon (exciting photon), resulting in a Stokes Raman scattering, as depicted in Figure 1b. The Stokes-shifted Raman spectrum (Figure 1b) is stronger than the anti-Stokes-shifted spectrum (Figure 1c), and both contain the same frequency information. The ratio of both spectra can provide information on temperature.

Vibrational energy and bond-stretching frequency are determined by several molecular properties, including atom types, atomic mass, molecular geometry, hydrogen bonding, and bond order (single bond vs double bond vs triple bond). It is important to recognize that Raman scattering measures molecular polarizability (the extent to which an electronic cloud can be distorted), as molecular vibrations can affect polarizability, providing useful information on molecular dipoles. Hence, both intramolecular and intermolecular vibrations are

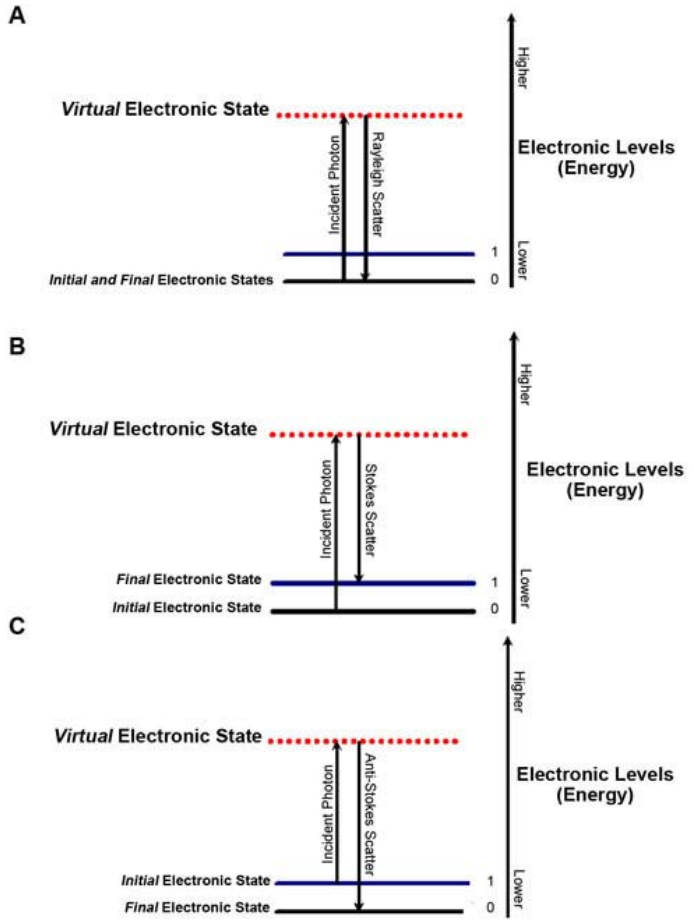

Figure 1. Principles of Raman scattering: (A) Rayleigh scattering; (B) Stokes Raman scattering; and (C) anti-Stokes Raman scattering.

Raman-active. The Raman-active vibration selection rule states that there must be a change in polarizability accompanying a vibration. In other words, strong Raman scattering occurs with a larger change in polarizability of distributed electron clouds, as found in a carbon-carbon double bond where the π-electron cloud is easily distorted because bond stretching and/or bending causes a significant change in the electron cloud density and induced-dipole moment. Hence, aromaticity is associated with strong symmetric vibration and a strong Raman band. Strong Raman scatters have symmetrical vibrations and include phenyl moieties and other aromatic moieties,[4] sulfide bonds, and carbon-carbon single and double bonds, which are all common structural characteristics of many pharmaceutical molecules. In contrast, the O-H bond is inherently highly polar because of the uneven distribution of the electron cloud favoring the oxygen atom; hence, polarizability is low and so is the Raman scattering. This is due to the fact that a highly polar moiety, such as the O-H bond, has a weak vibration and low Raman band, which is ideal for aqueous systems.

It is noted that infrared (IR) spectroscopy is also commonly used in molecular characterization of pharmaceutical materials, as it is complementary to Raman spectroscopy; however, sample preparation is required. Another benefit of Raman is that there tends to be less spectral overlap with common pharmaceutical excipients.[5] Additionally, pharmaceutical drug product containers (eg, glass and plastic) absorb mid-IR light due mainly to C-H vibrations, so noninvasive drug product identification and on-line process (in situ) monitoring is not possible with IR, as it is with Raman spectroscopy (to be discussed below).[6] Unlike Raman spectroscopy (symmetric vibration), IR requires a dipole moment change (ie, asymmetric vibration). Accordingly, weak Raman scatters tend to be strong IR absorbers and include bond vibrations present in polar moieties, such as carbonyl and hydrogen-bonded hydroxyl groups, since they display asymmetric (IR) rather than symmetric (Raman) vibrations. The various types of Raman spectroscopy and their applications are summarized in Table 1.

Several excellent reviews[7-9] discuss in detail the Raman effect, the various types of Raman spectroscopy, Raman band frequencies,[10,11] and the many applications of Raman spectroscopy in chemistry, biology, material science, and medicine. Raman spectroscopy can provide important information on molecular composition, structure, conformation, the degree of order and/or disorder, phases and phase transitions,

Table 1. Types of Raman Systems and Their Applications in the Characterization and Analysis of Pharmaceutical, Biocolloidal, and Aerosol Systems

Type of Laser Scanning Raman	Analytical Application
Fourier transform Raman spectroscopy	Common method used in process, quality, and quantity control applications in pharmaceutical systems
Raman microspectroscopy	Chemical imaging and mapping
UV resonance Raman spectroscopy	Polypeptide and biopolymer secondary structure and conformational transitions
Surface-enhanced Raman spectroscopy	Colloidal dispersions, molecular self-assemblies, inclusion complexes, nanoparticles, surfaces, and monolayers; chemical sensing biochemical analysis; rheology and gelation of hydrogels; interfacial molecular interactions
Resonance-enhanced Raman spectroscopy	Specific analysis of a material existing within a complex or mixture of materials
Red-excitation dispersive Raman spectroscopy	Respirable pharmaceutical powders for pulmonary inhalation aerosol delivery
Linear Raman spectroscopy	Aqueous aerosols

inter- and intramolecular interactions, hydrogen bonding, polymorphs, hydrates, anhydrates, molecular conformation, and polymer chain conformation. The purpose of this review is to highlight the main types of Raman spectroscopy and Raman microscopy (chemical imaging) techniques that have been successfully employed in the pharmaceutical sciences, with an emphasis on biocolloidal self-assemblies, nonaerosol drug delivery systems, and pulmonary inhalation aerosols. Additionally, this review will describe in detail the reports of Raman applications in pulmonary medicine and pharmaceutical inhalation aerosols demonstrating the potential for routine application of this powerful analytical and imaging technique in the molecular and surface characterization of inhalation aerosol delivery systems.

Types of Raman Spectroscopy

Fourier Transform Raman Spectroscopy

Fourier transform Raman (FT-Raman), the Raman method commonly used in pharmaceutical systems, prevents fluorescent background by using a longer wavelength in the near-IR region (typically 1064 nm).[12] Its success in routine pharmaceutical analysis can be attributed to its specificity (molecular fingerprint), reliability, efficiency, and cost-effectiveness as a quantitative method compared with high-pressure liquid chromatography, which always requires sample pretreatment and the use of solvents. Furthermore, it is a nondestructive and noninvasive biochemical analytical method.

Resonance-Enhanced Raman Spectroscopy

Resonance-enhanced Raman spectroscopy (RERS) occurs if the wavelength of the incoming exciting laser is near or within the electronic energy spectrum of the sample molecule, causing a resonance enhancement in the intensity of molecular vibrations. This is in contrast to conventional Raman spectroscopy, where, according to scattering theory, the wavelength of the incoming exciting laser is far below the first electronic transitions. This Raman method[13] has also been used extensively in pharmaceutical systems. Accuracy, precision, and enhanced sensitivity are all advantages in RERS.

Surface-Enhanced Raman Spectroscopy

In an effort to overcome the inherently weak Raman signals in conventional Raman methods and the ever-present problem of fluorescence of many API materials, surface-enhanced Raman spectroscopy (SERS) provides stronger Raman signals by taking advantage of electromagnetic enhancement and charge-transfer states. SERS[14] is quite useful in the study of biocolloidal dispersions (Figure 2), biomonomolecular layers (monolayers/nanolayers) of materials and their surfaces, including biomimetic models, biopolymers, inclusion

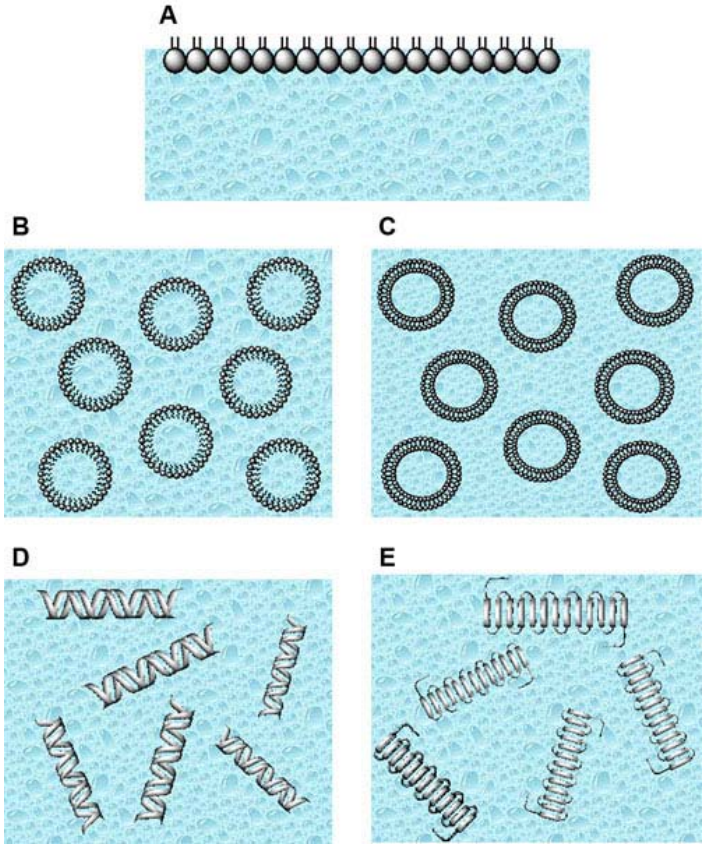

Figure 2. Aqueous dispersions of biocolloidal self-assemblies studied by Raman spectroscopy: (A) phospholipid monomolecular layers (nanolayers) at the air-water interface; (B) micelles; (C) liposomes; (C) DNA; and (E) helical protein.

complexes, living cells, nanoparticles, and pharmaceutical materials. Unique applications of SERS include colloidal dispersions, molecular self-assemblies, DNA/RNA mononucleotides,[15] oligonucleotides, nanoparticles, surfaces, monolayers, chemical sensing, biochemical analysis, biomedical diagnostics,[16] rheology and gelation of hydrogels,[17] biopolymer surface orientation, membrane transport processes,[18] colloidal nanostructures,[19] bacterial cells, single living cell uptake of nanoparticles,[20] and interfacial molecular interactions. Surface-enhanced hyper-Raman scattering incorporates 2-photon excitation with SERS, enabling the investigation of nanoparticles with single biological cells.[21]

Raman Chemical Imaging of Biocolloidal Self-Assemblies and Nonaerosol Pharmaceutical Delivery Systems

In general pharmaceutical analysis, Raman spectroscopy[22] is a real-time, noncontact, and noninvasive analytical technique in the chemical analysis, characterization, and quantification of various structures, metastable phases, molecular interactions, and reactivity in pharmaceutical solid dosage forms and powders[5,8,9,12,23-26] with minimal sample preparation.

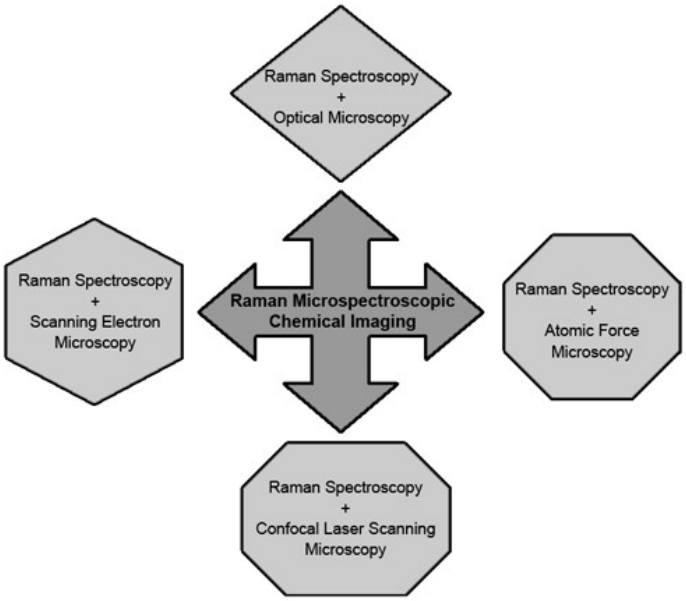

Figure 3. Various types of Raman microspectroscopic chemical imaging.

Raman chemical imaging (Figure 3) using Raman microscopy provides nondestructive, noninvasive molecular imaging capability without the use of fluorescent dyes or external markers. These advantages have vastly expanded Raman capabilities to biomacromolecular self-assemblies (eg, nucleic acid complexes and viruses),[27,28] shown in Figure 2, and biological media (eg, cell-based assays), with considerable application to in vitro and in vivo pharmaceutical science research.[24,29] Incorporating an optical microscope and motorized stage into the Raman instrument for spectroscopic chemical imaging by obtaining spectra for a defined 2-dimensional area with a resolution down to 1 μm[12] has further expanded Raman spectroscopy's utility in various structural and molecular investigations. These direct and quantitative Raman chemical imaging (Figure 3) and mapping (Figure 4) investigations include biomaterial nanotubes (providing a spatial resolution of ~25 nm),[30] drug-polymer-controlled drug delivery systems,[31,32] solid-state polymorphic transformations,[33-37] and drug disposition research.[24,38-42] The combination of scanning electron microscopy (SEM) and Raman spectroscopy has been applied in single-crystal hydration studies of carbamazepine, in the absence and presence of excipients, where it was demonstrated that defect structures were of greater importance in the initiation of the hydration process than the crystal face.[43]

Unlabeled and unfixed single living cells and organelles can be molecularly examined rapidly, noninvasively, and nondestructively by Raman chemical imaging. This novel technique has great potential in medical applications (ex vivo and in vivo),[44] tissue engineering, and drug discovery by virtue of its noninvasive, nondestructive, and rapid molecular fingerprinting of the effects of pharmaceuticals on single living cells at various stages of the cell cycle, with detailed nanometer spatial resolution.[45] Raman chemical imaging has been used in cell biology,[46,47] dipalmitoylphosphatidylcholine (DPPC)/cholesterol vesicle bilayer phase behavior,[48] differential tissue histopathology and chemical composition variation for cancer detection and degree of cancer progression in different tissue types,[47,49-53] and identification of and differentiation between multidrug-resistant cancer cells.[54]

Recently, laser scanning confocal microscopy imaging and Raman spectroscopy have been demonstrated to be very useful in noninvasive mapping (Figure 4) of chemical properties with high-resolution images, including 3-dimensional (3-D) views. The advantages of a confocal optical setup are (1) reduced unwanted background signals, (2) enhanced contrast, (3) stacking, and (4) depth information via 3-D imaging resulting in high spatial and temporal resolution. Differences in chemical composition not seen in the optical image become directly apparent in the Raman image. In addition, this nondestructive imaging of chemical properties and phases is performed without extensive or special sample preparation. In sophisticated setups, complete spectra can be obtained for each image pixel, and, conversely, images can be obtained on certain parts of interest in the Raman spectrum. Confocal Raman microspectroscopy[55] has been reported to have great potential for efficiency in assessing and quantifying the physical state of a drug, physicochemical stability of the formulation, content, and homogeneity of drug distribution in a polymer formulation matrix.[56] Additionally, confocal Raman microspectroscopy has been employed in protein crystallization,[57] molecular imaging of the effects of penetration enhancers and drugs on in vivo human stratum corneum,[58-60] and in vivo human skin analysis.[61] With an elegant combination of confocal Raman spectroscopy with laser tweezers (ie, optical trapping to isolate single cells in a more natural state, as opposed to adsorption onto the surface of a solid substrate,

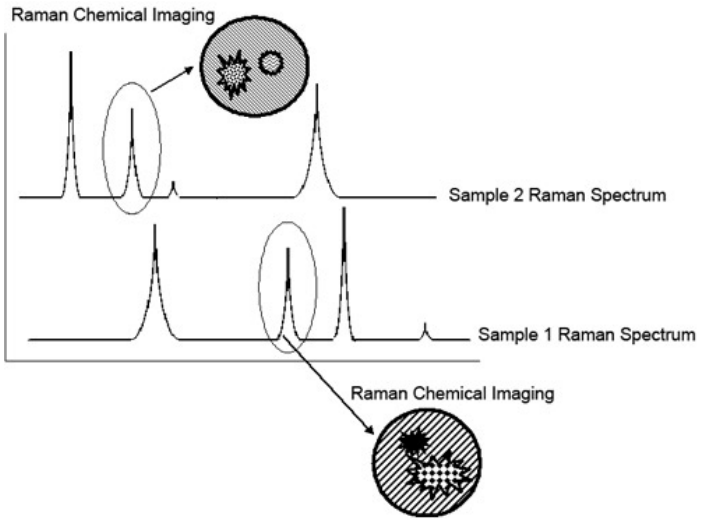

Figure 4. Schematic of Raman mapping.

which is known to disturb the natural state), rapid identification of single live cells (bacterial cells and fungal spores) and organelles can be accomplished from every angle.[62-64] Additionally, efforts are being made in expanding laser tweezer confocal Raman molecular application to single live cell cancer screening with a 98.3% cancer detection sensitivity based on intrinsic characteristic biomolecular differences (as opposed to physical attributes, eg, surface phenotype) in single live transformed lymphocytes and normal human lymphocytes.[65] Laser tweezer Raman spectroscopy has been used in investigating the activation of individual T cells[66] and the dynamic real-time effects of alcohol on a single living red blood cell.[67]

Raman microscopy 3-D profiling has been performed with atomic force microscopy (AFM) phase imaging with confocal Raman microscopy to successfully identify and analyze, at the nanometer level, the distribution of amorphous regions on the surface of semicrystalline solid pharmaceutical excipients.[68] It was shown that Raman spectroscopy can complement AFM and can provide micrometer-level information (with lateral spatial resolution on the order of 1-2 μm)[69] on the depth of the surface amorphous domains, particularly as it applies to semicrystalline particles, in addition to characterizing bonding interactions and quantifying amorphicity/degree of crystallinity content. In addition, confocal Raman microimaging of pharmaceutical coatings in conjunction with AFM analysis has been reported in identifying the chemical composition of small areas of the coating.[70]

Disadvantages of classical Raman spectroscopy, in the context of pharmaceutical applications, are fluorescence in the sample interfering with Raman scatter detectability and the inherently weak Raman scattering process, resulting in low sensitivity and the need for sensitive detectors and intense laser excitation sources.[23] SERS[16,23,71] overcomes these limitations by providing high sensitivity and hence is a powerful analytical technique for biocolloidal systems, antibiotic drug adsorption,[72] precise drug detection and quantification in bodily fluids,[73] and antiretroviral[74,75] and antitubercle bacillus drug[76] molecular conformational investigations. Using a combination of micro-Raman and SERS, the recognition process of drugs with large biomolecules (eg, albumin) through the use of colloidal nanoparticles was reported through investigation of the binding properties of the drugs with albumin.[77] Surface-enhanced Raman microscopy has been successfully used in imaging of live cells,[78] including individual human lymphocyte cells.[79] SERS-confocal microscopy has been used in chemical imaging of cellular proteins, including enzymes, cellular proteins, and receptors in single cells.[80] Surface-enhanced micro-Raman spectroscopy in model diagnostic systems incorporating microfluidics[81] showed potentially promising application in pharmaceutical research and clinical chemistry. Bacterial discrimination[82] via SEM-SERS, and viral detection in immunoassays[83] and DNA nanoimaging[84] via SERS-AFM, have been recently reported. A novel chemical nanoimaging technique combines SERS with AFM (tapping mode) to provide highly detailed spectra and high-resolution chemical imaging of biological materials, including bacterial cells and DNA bases.[85]

Raman Applications in Pulmonary Systems and Pharmaceutical Inhalation Aerosols

Atmospheric polluting particulate matter, consisting of polyaromatic hydrocarbons and particulate soot, and its relationship to pulmonary diseases (ie, pneumonia, asthma, chronic obstructive pulmonary disease, and lung cancer), global climate change, and oceanic warming have been the subject of intense research for many decades. This is especially true in recent years, when "molecular fingerprint" characterization tools, such as Raman chemical imaging and mapping (Figures 3 and 4, respectively), have revealed demonstrated utility in atmospheric aerosol and bioaerosol research. Much attention has been given to bioaerosols and their relationship to various types of pulmonary allergic and infectious diseases. Additionally, the topic of infectious bioaerosols is gaining particular attention in the context of biodefense and global public health. Based on the successes of Raman spectroscopy in atmospheric and bioaerosol research, Raman applications for the respiratory system and pharmaceutical inhalation aerosols are being increasingly reported. As will be revealed in the following discussion, Raman spectroscopy has great promise for vast and powerful application in therapeutic inhalation aerosols, pulmonary histopathology, pulmonary infectious diseases, pulmonary immunology, lung surfactant biophysics and interfacial phenomena, and respiratory molecular biology.

Raman Spectroscopy in Atmospheric Aerosols and Aerosol Particulate Reactions

Raman spectroscopy has been traditionally employed in investigating and characterizing single aerosol particles,[86,87] atmospheric aerosol particles,[88] and microparticle multicomponent aerosols.[89] Raman spectroscopy has been applied to successful in situ measurement of the chemical compositions of monodisperse and polydisperse aerosols in the micrometer size range with a low signal-to-noise ratio.[90] In situ chemical analysis of ambient uncharged atmospheric aerosol particles with diameters > 1 μm was captured using an electrodynamic balance and levitated while Raman spectroscopy with a charge-coupled device (CCD) detector was successfully employed to identify chemical substances in the aerosol particles.[91] Raman chemical imaging using SEM and confocal laser scanning microscopy (CLSM) has also been used in the mapping of fine particulate atmospheric aerosols,[92,93] mass and heat transfer effects on evaporating aerosol droplets,[94,95] aerosol water droplet growth,[96,97] single aerosol droplet physical and chemical dynamics,[98] gas-aerosol chemical reactions involving

water vapor and greenhouse gases,[99-103] aerosol chemical reactions in the synthesis of polymeric microspheres,[104] and interfacial hydrogen bonding in water aerosols.[105] As seen with nonaerosol systems, enhanced Raman scattering signal was observed in aerosol chemicals analyzed by resonance Raman spectroscopy.[106] Raman microspectroscopy (Figure 3) has enabled the imaging and molecular fingerprinting (Figure 4) of hydrocarbon-water mixing during multicomponent aerosol particle formation.[107]

Raman Investigations of Bioaerosols

Raman characterization of bioaerosols, such as pollen, viruses, and bacteria, that are regularly inhaled and can cause and exacerbate pulmonary diseases has been reported.[108-110] Aerosolized aqueous suspensions of bioaerosols containing *Escherichia coli, Pseudomonas aeruginosa,* and *Salmonella typhimurium* have been examined using SERS.[111] Infectious bioaerosolized pathogens acquired by the pulmonary route have been the subject of much interest in global public health and biodefense. Bioaerosols consisting of aerosolized nanocolloidal suspensions of pollen,[112]*E coli,*[112]*Bacillus anthracis* (anthrax),[113]*Francisella tularensis* (tularemia),[113] and *Bacillus subtilis* (anthrax spores)[114] have been successfully detected at low levels and molecularly characterized by Raman chemical imaging and SERS.

Raman Studies of the Respiratory System

As mentioned previously, antimicrobial drugs used in the treatment of the pulmonary infection tuberculosis have been investigated using SERS.[76] Additionally, the various parts of the pulmonary system have been investigated using Raman spectroscopy. The interfacial properties and molecular interactions (ie, electrostatic, hydrophobic, hydrogen bonding, and van der Waals) of human lung surfactant models containing DPPC, and/or palmitoyloleoylphosphatidylglycerol (POPG), with synthetic cationic hydrophobic heteropolypeptide surfactant derivatives of human surfactant protein SP-B were deciphered by quantitative Raman interaction parameters reported by Vincent et al.[115] Additionally, they found using model human lung surfactant systems of DPPC mixed with DPPG (dipalmitoylphosphatidylglycerol) that specific lipid-heteropolypeptide interactions result in a dynamic bilayer microdomain heterogeneity[116] that is necessary for the normal mechanics of pulmonary respiration.

Various types of immortal and mortal pulmonary cell lines have been employed in many in vitro models of pulmonary transport and absorption studies of pulmonary aerosol and particulate uptake.[117]

In an effort to apply powerful spectroscopic and chemical imaging techniques in the study and molecular characterization of the pulmonary system at the cellular and subcellular levels, in very recent years, Raman spectroscopy has just begun to demonstrate its unique and vast utility in noninvasive and nondestructive in vitro and in vivo pulmonary cell and subcellular applications. The molecular structure of cellular components of single lung fibroblast cells (without labeling) under stress followed by apoptosis has been examined by Raman mapping.[118] In an unlabeled single cell undergoing apoptosis, it was demonstrated that the Raman band intensity of the nucleic acids present in the nucleus and cytoplasm decreased as the number of cell surface blisters (having higher nucleic acid content) increased, which was indicative of nucleus degradation.[118] It was reported by Kaminaka et al[119,120] that Raman spectroscopy of human lung tissue (normal and cancerous) demonstrated that 2 strong vibrational bands at 1666 and 1448 cm^{-1}, representing collagen, increased in lung tissues upon lung cancer progression (as noted in other cancerous tissue systems) and hence can be used as a Raman marker in diagnosis.

The molecular composition and histological evaluation of normal human bronchial tissue was characterized in situ by Raman mapping, as reported by Koljenovic et al,[121] who sought to have a biochemical and molecular understanding of lung cancer. They found that the spectra of bronchial mucus, which has relatively high quantities of triolein, were dominated by strong lipid signals, and strong collagen and glycosaminoglycan signals were associated with cartilage. Relatively lower lipid and higher DNA signals were associated with the basal side of the bronchial epithelium.

It was shown that formalin, which preserves normal and malignant human bronchial tissues, does significantly and adversely affect the Raman spectra of these tissues through the introduction of artifacts; and hence, when using fixed tissue, thorough rinsing in phosphate-buffered saline may assist in obtaining more meaningful Raman spectra.[122,123] The authors found that formalin fixation did not affect the major Raman signals for lipids and proteins, but the Raman intensities did decrease upon formalin fixation compared with fresh unfixed human bronchial tissue. This decrease was suggested to be associated with the effect of formalin on the bronchial lipid self-assembly. In tumor tissue, the same trend was reported, particularly for the porphyrin (hemoglobin from the blood) and water Raman bands, as it related to the state of hydration of the lung tissue samples. For Raman lung tissue studies for molecular characterization of normal and lung cancer states, the authors recommended using fresh tissue rather than formalin-fixed tissue or in vivo Raman analysis.

In one study using Raman spectroscopy on fresh (unfixed and never frozen) lung tissue using normal and malignant lung tissue it was found that the normalized Raman phospholipid band intensities decreased and the amide I and amide III vibrational bands increased in lung cancer

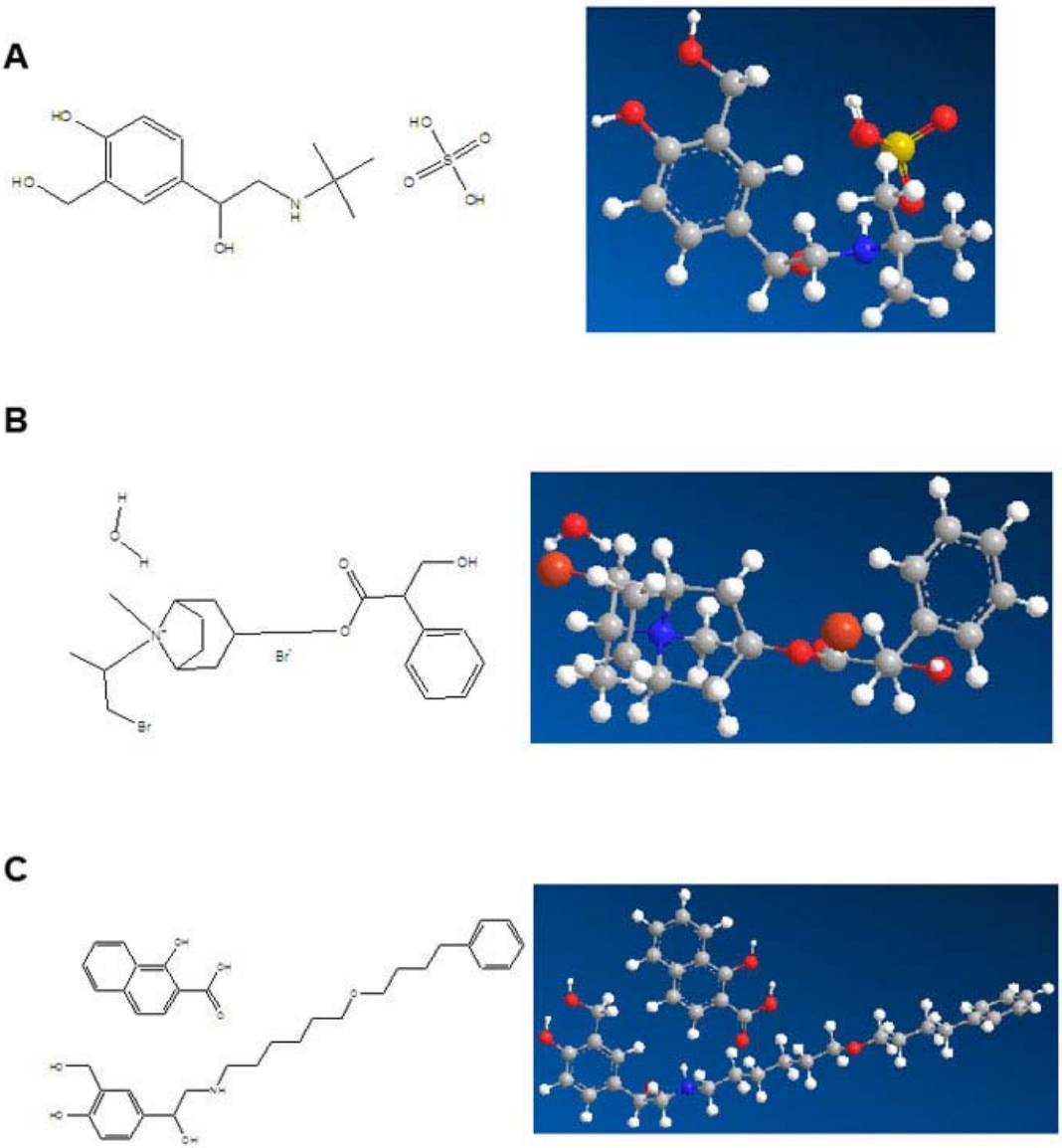

Figure 5. Chemical structures and molecular modeling of various pulmonary β-agonist and anticholinergic drugs that have been studied by Raman spectroscopy: (A) albuterol sulfate (short-acting β-agonist); (B) ipratropium bromide monohydrate (anticholinergic); and (C) salmeterol xinafoate (long-acting β_2-agonist).

development[123,124] as the protein content increased and protein conformational changes occurred, accompanied by increased nucleic acid content. The authors suggest that this can be attributed to the very unique organ structure of the lungs: compared with other organs, the lungs are less dense, with relatively small amounts of protein, and the density increases as the protein content increases (ie, amide I band) during disease progression.

Raman Investigations of Pharmaceutical Inhalation Aerosols

Raman spectroscopy and chemical imaging is beginning to find increasing application in the molecular characterization of pharmaceutical aerosols[125-127] for pulmonary delivery, and in particular, dry powder inhalation aerosol delivery systems.[117,128,129] Depicted in Figures 5 and 6, respectively, are the chemical structures (ChemDraw Ultra 10.0, ChemOffice 2006, Cambridgesoft, Cambridge, MA) and molecular modeling (Chem 3DPro 10.0, ChemOffice 2006, Cambridgesoft) of the pulmonary drugs that have been characterized by Raman spectroscopy. Similarly, Figure 7 shows the chemical structures and molecular modeling of pulmonary inhalation aerosol carriers and excipients. The crystallinity, polymorphism, and amorphicity of α-lactose monohydrate (Figure 7a), the only US Food and Drug Administration–approved carrier for use in dry powder pharmaceutical aerosols, have been analyzed and distinguished using Raman spectroscopy.[130-133] The molecular nature of salbutamol (albuterol) sulfate[134] (Figure 5a) and salts crystallized from

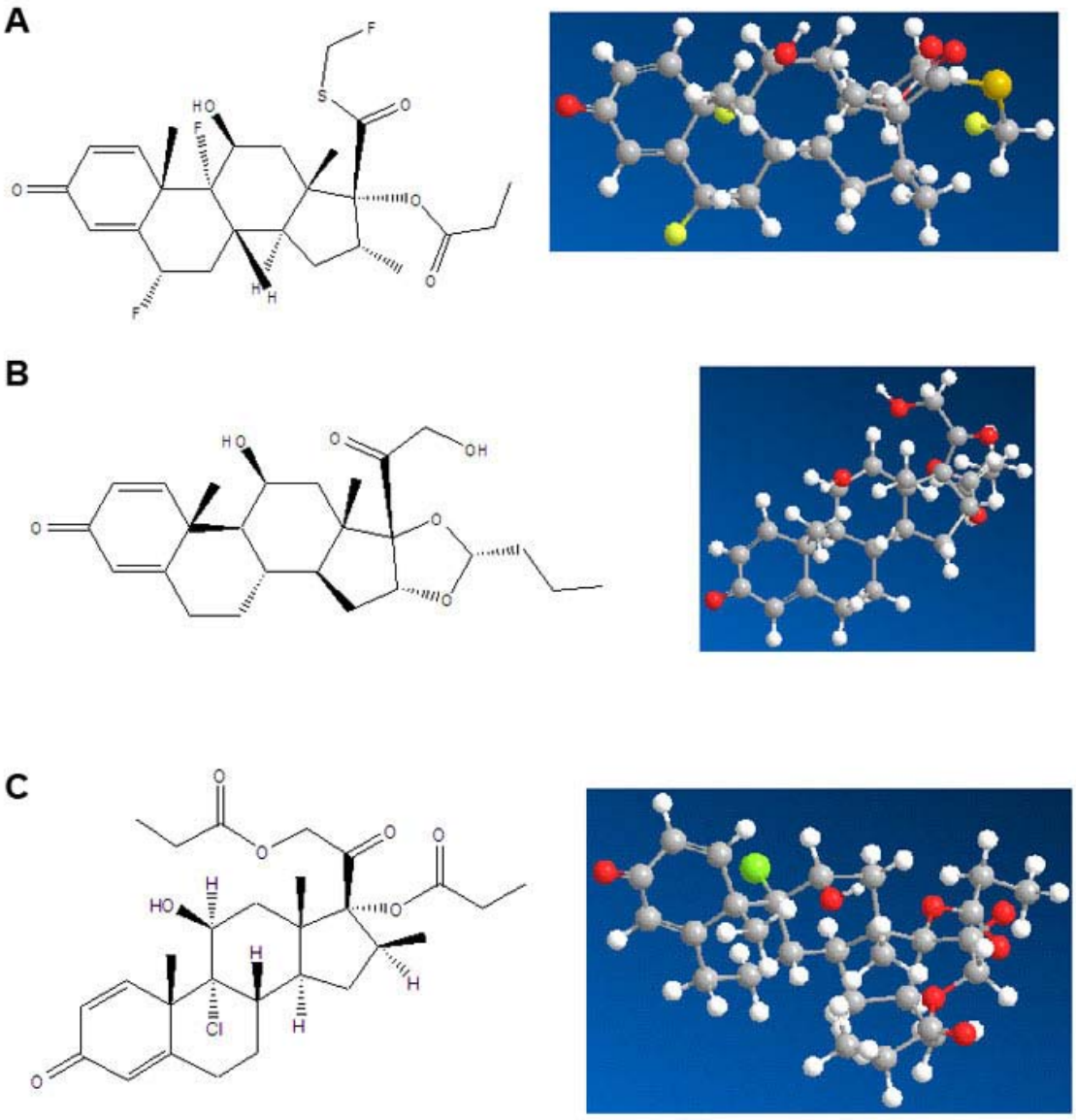

Figure 6. Chemical structures and molecular modeling of various pulmonary corticosteroid drugs that have been studied by Raman spectroscopy: (A) fluticasone propionate; (B) budesonide; and (C) beclomethasone dipropionate.

salbutamol base[135] has been examined using Raman spectroscopy. Particle engineering techniques such as supercritical fluid (SCF) technology, solution-enhanced dispersion with supercritical fluids (SEDS), supercritical fluid extraction of emulsions, and spray-drying are used often in intelligently designing respirable dry powder particles, as described in detail by Hickey and Mansour.[117]Figure 8 illustrates the general phase diagram of an SCF, which is liquefied gas existing as a single phase above its critical point, T_c, and possessing desirable properties of both its liquid (L) state and its gaseous (G) state.[117] It was reported[136] that SEDS-produced lysozyme retained biological activity as a respirable solid particle while exhibiting minor changes in its FT-Raman spectra.

Lysozyme has often been used as a robust model protein in biotherapeutic drug delivery, including dry powder inhalation aerosols for dry powder inhalers (DPIs) and aerosol propellant systems for metered-dose inhalers (MDIs). Quinn et al[137,138] investigated the biomolecular structural conformational stability of lysozyme (predominantly α-helical conformation) and deoxyribonuclease I (predominantly β-sheet conformation) in the hydrofluoroalkane (HFA) propellants (7.5% wt/wt) tetrafluoroethane (HFA 134a) and heptafluoropropane (HFA 227) at 25°C, using FT-Raman consisting of an Nd^{3+}:YAG laser at 1064 nm with a laser power of 500 mW for solids and 800 mW for suspensions. Following actuation, both proteins maintained enzymatic activity at 85% and 90% for DNase I in HFA 227 and HFA 134a, respectively, and at 94% and 91% for lysozyme in HFA 227 and HFA 134a, respectively.[137] FT-Raman provided molecular information related to secondary structure. For lysozyme structural stability in the solid state and as an aqueous

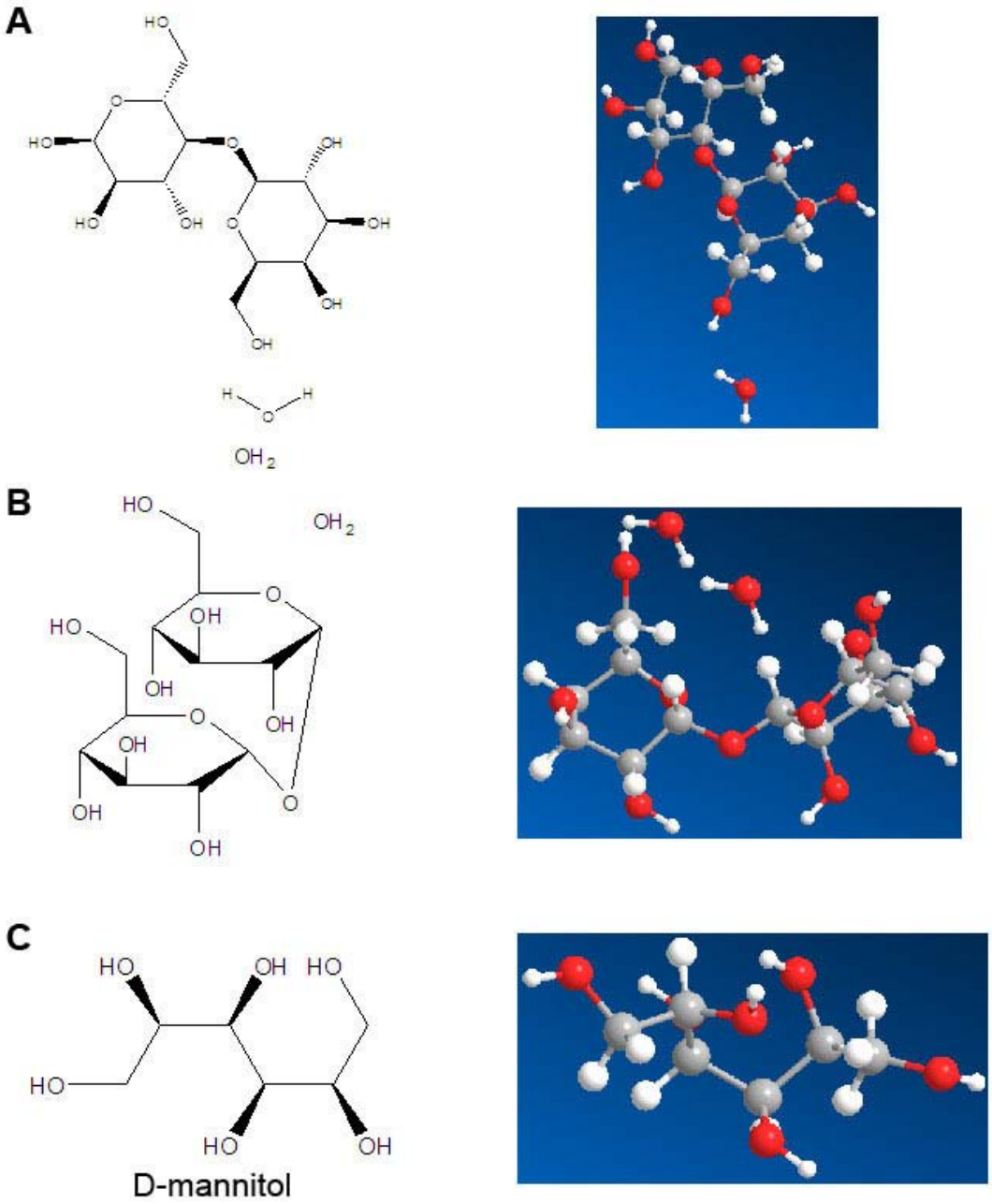

Figure 7. Chemical structures and molecular modeling of carriers and excipients used in pulmonary aerosol inhalation delivery systems that have been studied by Raman spectroscopy: (A) lactose monohydrate; (B) trehalose dihydrate; and (C) D-mannitol.

solution, no significant changes were observed in the C-C band (~900 cm^{-1}), the characteristic amide I band (1660 cm^{-1}), the amide III band between 1264 cm^{-1} and 1300 cm^{-1} that characterized lysozyme's α-helical structure, and the disulfide band (~507 cm^{-1}) that characterized a *gauche-gauche-gauche* conformation.[138] The strongest propellant marker peaks were at 857 cm^{-1} and 839 cm^{-1} for HFA 227 and HFA 134a, respectively. Lysozyme maintained its structure in these propellants, as indicated from the FT-Raman spectra collected through glass vials, wherein the amide I band (1660 cm^{-1}) and C-C band (900 cm^{-1} and 930 cm^{-1}) did not change significantly. However, the amide III band exhibited a decrease in intensity, and the authors attributed this to the effect of the local environment (aqueous vs nonaqueous propellant) on the peptide backbone conformation.

Raman spectroscopy was employed by Dem et al[126] in tracking crystallization in a droplet of mannitol (Figure 7c) during spray-drying by monitoring polymorphism in situ. The Raman instrument (Nd: YAG laser at 532 nm) was equipped with an electrodynamic trap (at a controlled relative humidity and temperature) where a single solid particle or droplet can be levitated in the center of the trap with a 785-nm laser. The aqueous mannitol droplets, which had a

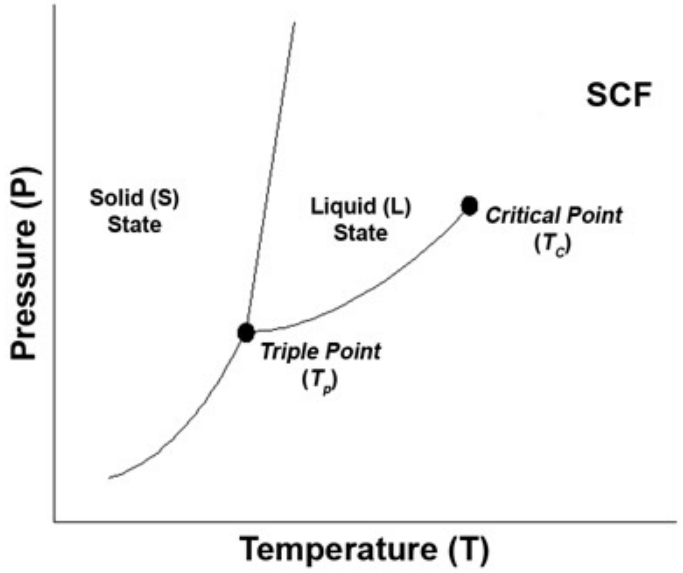

Figure 8. Phase diagram depicting the SCF region, the 2-phase equilibria (coexistence) boundary lines, the triple point, T_p, and the critical point, T_c. The SCF region is above T_c where a single-phase liquefied gas exists. SCF indicates supercritical fluid.

diameter of 90 μm, were then charged prior to entering the trap. Single-particle Raman spectroscopy distinguished between 3 mannitol polymorphic forms during droplet evaporation at various relative humidities and temperatures, and a polymorphic phase diagram with boundary lines was constructed.[126]

Dispersive Raman imaging was reported[139] in determining the particle size distribution of the commercially available combination product MDI, Combivent, which simultaneously delivers the pulmonary drugs ipratropium bromide (Figure 5b), an anticholinergic, and albuterol sulfate (Figure 5a), a short-acting β-agonist, in 1 actuation. The Raman peaks monitored were at 985 cm^{-1} and 1014 cm^{-1} for albuterol sulfate and ipratropium bromide, respectively, and the spectral range of 960 to 1040 cm^{-1} was used in Raman imaging (68-mW laser power and 100× objective) of particles following 1 actuation and propellant evaporation. The spatial resolution was ~250 nm. Raman imaging has found utility in the identification of foreign particles in a dry powder inhalation product, as reported by Kreher et al,[125] in 3 size ranges. It was found that complementary information on chemical composition was obtained for most DPI particles by SEM/X-microanalysis and Raman microprobe, and Raman-identified organics such as carbohydrates, long-chain hydrocarbons, polyethylene, and polyvinylacetal moieties in the DPI particles.[125]

Dispersive Raman chemical imaging has been successfully used to determine the chemical identity and particle size distribution of active drug (eg, beclomethasone dipropionate, as shown in Figure 6c) from among inactive compounds (carboxymethylcellulose sodium, microcrystalline cellulose, polysorbate 80, dextrose, phenylethyl alcohol, and benzalkonium chloride) in suspension-based aerosols and aqueous suspension nasal sprays containing high-dose corticosteroid, such as the commercially available nasal spray product Beconase AQ.[140,141] Beconase AQ was used as the control, and 5 formulated aqueous nasal spray suspensions were used in the blind study. Full Raman spectra were obtained for the aqueous suspension containing corticosteroid and excipients, and chemical imaging revealed the optimal characteristic drug peak marker at 1662 cm^{-1} that clearly distinguished the active drug from the excipients. Particle size and shape of the drug was determined from Raman chemical imaging of dry deposits following actuation deposition onto aluminum-coated glass microscope slides.

It has been reported that red-excitation dispersive Raman spectroscopy can be applied to quantify polymorphism and amorphous content in a multicomponent dry powder formulation consisting of spray-dried mixtures of salmon calcitonin and mannitol[142] and in the study of the physical stability of these dry powder inhalation systems.[143] This technique of combining red diode laser excitation with dispersive Raman spectroscopy provides enhanced signal-to-noise ratio, higher sensitivity, and less sample heating compared with FT or dispersive Raman spectroscopy.[142] Combining a sensitive Raman system with visible excitation provides an enhanced signal-to-noise ratio, and the fluorescence background caused by visible excitation is not a limitation (as it is for biological applications) for pharmaceutical materials (excipients, biopolymers, proteins) owing to their high purity. These dry powder aerosols were analyzed by a diode laser operating at a wavelength of 669.85 nm, at a power of 250 mW, and with a spectral bandwidth of 1 cm^{-1}. The digital sensor was composed of a cryogenically cooled CCD system. This particular Raman system was equipped with an aluminum cavity (1-μL volume) for a 100 to 800 μg sample such that scattered laser radiation could be reflected back into the powder sample, leading to improved signal.

Raman spectroscopy has been used on not only dry powder aerosols but also aqueous aerosol particles and propellant-based aerosol systems. Stimulated Raman scattering has been used to characterize aqueous aerosols by linear Raman spectroscopy.[144] Scanning near-IR Raman microscopy has been successfully used to map aerosol particulate deposits on the stages of an Anderson cascade impactor (ACI), as shown in Figure 9, from a combination pressurized MDI (pMDI), Ventide.[145] ACI is the standard in vitro model of aerosol deposition in the lungs. A thorough understanding of the deposition profiles can be achieved through physicochemical investigations into the molecular and surface interactions occurring in the pulmonary inhalation aerosol delivery system (stability, adhesion, agglomeration, etc) as a function of particle size fractions based on the ACI stage deposition profiles. Aerosol deposits on stages 3 and 5

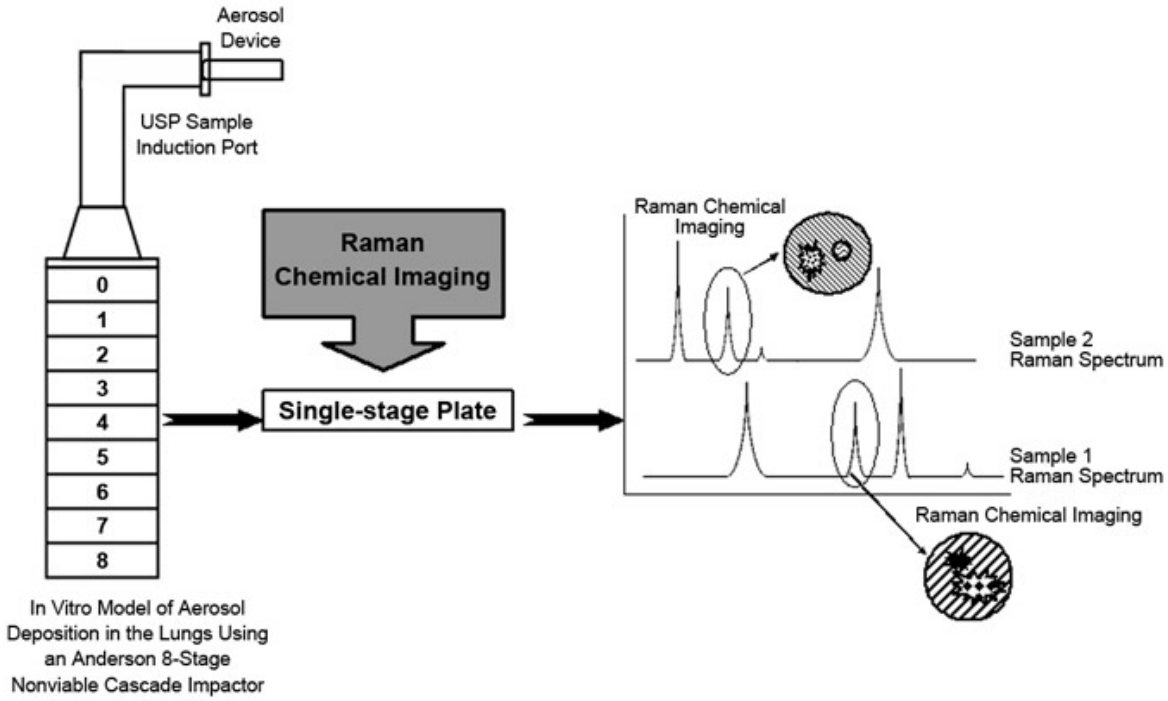

Figure 9. Schematic of Raman mapping of pharmaceutical inhalation aerosols. USP indicates US Pharmacopeia.

following a single Ventide pMDI actuation were used in Raman mapping. The Raman system used a high-performance near-IR 785-nm laser, and 10 mW of total laser energy was directed to the sample for a 30-second time scan from 1338 cm^{-1} to 1829 cm^{-1}. Raman maps were 100 × 100 μm in area, where Raman bands at 1610 cm^{-1} and 1662 cm^{-1} represented salbutamol and budesonide dipropionate, respectively. It was reported that these Raman bands for the drugs exhibited minimal interference from the pMDI excipients. Good correlation was reported between the Raman maps of the ACI plate stages and chemical analysis of the stages. Raman mapping of the stages confirmed that no new molecular bond formation (indicative of chemical degradation) in the 2 drugs occurred, based on the absence of new peaks and drug peak shifts. The authors reported that even though oleic acid may be present as a thin film on the stages, it could not be detected by Raman spectroscopy, presumably because of its low concentration, which was lower than the limit of detection.

In addition to Raman chemical imaging of combination MDI products containing an anticholinergic and a short-acting β-agonist, combination inhaled products containing a long-acting β2-agonist and a corticosteroid have been investigated. Seretide MDI is a commercially available combination MDI product delivering fluticasone propionate (Figure 6a), a corticosteroid, and salmeterol xinafoate (Figure 5c), a long-acting selective β2-agonist, in the treatment of asthma. Asthma is a complex disease state that exhibits both bronchoconstriction and airway inflammation.[146] A long-standing interest in pulmonary inhalation aerosol delivery in the treatment of asthma is the clinical observation that combination products are more efficacious than separate administration of the 2 component drugs. Perhaps this may be a result of simultaneous codeposition of both drugs on a cell via a single inhaler in a single actuation in the same inspiratory breath. Moreover, codeposition may enhance synergistic drug effects. In an effort to gain insight into this, Theophilus et al[147] investigated the deposition per actuation from the commercially available combination and single MDI products Seretide (50 μg fluticasone propionate and 25 μg salmeterol), Serevent (25 μg salmeterol), and Flixotide (50 μg fluticasone propionate). Being an in vitro size model of the central airways, Plate 4 of the ACI, having a size range of 2.1 to 3.3 μm, was analyzed by Raman spectroscopy following MDI actuation at a flow rate of 28.3 L/min. The Raman microscope setup consisted of a 100× objective lens, a confocal hole set at 65 μm, and a cooled CCD detector connected to a 785-nm diode laser operating at 500 mW of laser power, which provided spatial resolution of ~3.2 μm. Raman chemical imaging was done on a 128 × 128 μm area. The authors showed from their Raman chemical images that the combination inhalation product delivered from a single device had significantly greater codeposition of both drugs, which suggested that the particles in the combination MDI are associated until the particles are deposited.[147] It was acknowledged that while the ACI is an in vitro model of pulmonary deposition, the differences observed in vitro would be expected to be much greater in vivo.[147] Propellant evaporation is a rapid, dynamic, and complex interfacial process where the

drug interaction with the propellant can have significant effects on final particle characteristics, including particle size, morphology, and deposition behavior. This particularly pertains to 2-drug MDI systems where coassociation between the 2 drugs can favorably occur within an aerosol propellant system, as has been previously reported[148] with salmeterol and fluticasone, and was demonstrated by Raman chemical imaging of codeposition.[147]

As we have recently reported, a comprehensive set of analytical techniques, including bulk and surface characterization methods, are necessary in the molecular characterization of microparticulate and nanoparticulate systems designed for pulmonary dry powder aerosol inhalation delivery.[117,128,129] The information on the molecular, surface, and interfacial properties that Raman characterization can provide is particularly important in applications related to respirable pharmaceutical powders, where understanding the molecular nature of these solid surfaces can enable their manipulation and tailoring for functionality at the nanometer level for targeted pulmonary delivery and deposition. Raman spectroscopy and chemical imaging are powerful analytical techniques, as detailed in this review, as they provide valuable molecular insight into a variety of biocolloidal self-assemblies and drug delivery systems, including inhalation aerosol drug delivery systems. Future Raman spectroscopy and chemical imaging investigations on pharmaceutical aerosols, particularly dry powder aerosol inhalation delivery systems, should examine the effects of temperature and relative humidity on hygroscopic particulate growth and in vitro aerosol performance, which are then correlated with phase transformations and in vitro deposition. Additionally, in vitro and in vivo Raman chemical imaging of microparticulate and nanoparticulate interactions with various living pulmonary epithelial cell types and pulmonary immune cells will provide valuable and needed biophysical insight into particulate uptake by living pulmonary cells and transport in the lungs. Moreover, Raman imaging in pulmonary medicine will enable a novel combination of molecular insight and noninvasive imaging capability that can molecularly characterize infected pulmonary cells, cancerous pulmonary cells, pulmonary disease states, and cellular delivery and disposition following pulmonary inhalation aerosol delivery.

CONCLUSIONS

As presented in this review, Raman mapping of aerosols at the micro- and nanometer level of resolution and correlation with in vitro aerosol lung deposition is now achievable with new, sophisticated, commercially available Raman microspectroscopy techniques. As has been demonstrated here, Raman chemical imaging has unique, noninvasive, and versatile applications in systems of pharmaceutical interest, and hence has vast potential for application in pulmonary inhalation aerosol research. Unique and important application potentials for Raman chemical imaging include aerosol deposition molecular profiling in the lungs and in specific individual pulmonary cells, and nondestructive chemical imaging of pulmonary aerosol inhalation delivery of biocolloidal self-assemblies and biotherapeutics, both in vitro and in vivo.

ACKNOWLEDGMENTS

Heidi M. Mansour gratefully acknowledges the generous financial support from the Pharmaceutical Manufacturers and Researchers of America Foundation for a Postdoctoral Fellowship Award in Pharmaceutics. Pfizer, Inc and DMV-Fonterra Excipients are thanked for their generous financial support.

REFERENCES

1. Raman CV. Anisotropy of molecules. *Nature.* 1922;109:75–76.

2. Raman CV, Krishnan KS. A new type of secondary radiation. *Nature.* 1928;121:501–502.

3. Singh RCV. Raman and the discovery of the Raman effect. *Phys Perspect.* 2002;4:399–420.

4. Tudor AM, Melia CD, Binns JS, Hendra PJ, Church S, Davies MC. The application of Fourier-transform Raman spectroscopy to the analysis of pharmaceuticals and biomaterials. *J Pharm Biomed Anal.* 1990;8:717–720.

5. Newman AW, Bryn SR. Solid-state analysis of the active pharmaceutical ingredient in drug products. *Drug Discov Today.* 2003;8:898–905.

6. McCreery RL, Horn AJ, Spencer J, Jefferson E. Noninvasive identification of materials inside USP vials with Raman spectroscopy and a Raman spectral library. *J Pharm Sci.* 1998;87:1–8.

7. Lyon LA, Keating CD, Fox AP, et al. Raman spectroscopy. *Anal Chem.* 1998;70:341–361.

8. Wartewig S, Neubert RH. Pharmaceutical applications of mid-IR and Raman spectroscopy. *Adv Drug Deliv Rev.* 2005;57:1144–1170.

9. Fini G. Applications of Raman spectroscopy to pharmacy. *J Raman Spectrosc.* 2004;35:335–337.

10. Dollish FR, Fateley WG, Bentley FF. *Characteristic Raman Frequencies of Organic Compounds.* New York, NY: Wiley-Interscience; 1974.

11. Lin-Vien D, Colthup NB, Fateley WG, Grasselli JG. *The Handbook of Infrared and Raman Characteristic Frequencies of Organic Molecules.* Oxford, UK: Elsevier Science & Technology Books; 1991.

12. Bugay D. Characterization of the solid-state: spectroscopic techniques. *Adv Drug Deliv Rev.* 2001;48:43–65.

13. Vickers TJ, Mann CK, Zhu J, Chong CK. Quantitative resonance Raman spectroscopy. *Appl Spectrosc Rev.* 1991;26:341–375.

14. Tian ZQ. Surface-enhanced Raman spectroscopy: advancements and applications. *J Raman Spectrosc.* 2005;36:466–470.

15. Bell SEJ, Sirimuthu NMS. Surface-enhanced Raman spectroscopy (SERS) for sub-micromolar detection of DNA/RNA mononucleotides. *J Am Cancer Soc.* 2006;128:15580–15581.

16. Vo-Dinh T, Yan F, Wabuyele MB. Surface-enhanced Raman scattering for biomedical diagnostics and molecular imaging. *Top Appl Phys.* 2006;103:409–426.

17. Miljanic S, Frkanec L, Biljan T, Meic Z, Zinic M. Surface-enhanced Raman scattering on molecular self-assembly in nanoparticle-hydrogel composite. *Langmuir.* 2006;22:9079–9081.

18. Wood E, Sutton C, Beezer AE, Creighton JA, Davis AF, Mitchell JC. Surface enhanced Raman scattering (SERS) study of membrane transport processes. *Int J Pharm.* 1997;154:115–118.

19. Aroca RF, Alvarez-Puebla RA, Pieczonka N, Sanchez-Cortez S, Garcia-Ramos JV. Surface-enhanced Raman scattering on colloidal nanostructures. *Adv Colloid Interface Sci.* 2005;116:45–61.

20. Kneipp J, Kneipp H, McLaughlin M, Brown D, Kneipp K. In vivo molecular probing of cellular compartments with gold nanoparticles and nanoaggregates. *Nano Lett.* 2006;6:2225–2231.

21. Kneipp J, Kneipp H, Kneipp K. Two-photon vibrational spectroscopy for biosciences based on surface-enhanced hyper-Raman scattering. *Proc Natl Acad Sci USA.* 2006;103:17149–17153.

22. USP. *<1120> Raman Spectrophotometry USP 29-NF 24 The United States Pharmacopoeia and The National Formulary: The Official Compendia of Standards*. Rockville, MD: US Pharmacopeial Convention; 2006:2983–2988.

23. Pinzaru SC, Pavel I, Leopold N, Kiefer W. Identification and characterization of pharmaceuticals using Raman and surface-enhanced Raman scattering. *J Raman Spectrosc.* 2004;35:338–346.

24. Huong PV. Drug analysis by Raman and micro-Raman spectroscopy. *J Pharm Biomed Anal.* 1986;4:811–823.

25. Vankeirsbilck T, Vercauteren A, Baeyens W, et al. Applications of Raman spectroscopy in pharmaceutical analysis. *TrAC.* 2002;21: 869–877.

26. Strachan CJ, Rades T, Gordon KC, Rantanen J. Raman spectroscopy for quantitative analysis of pharmaceutical solids. *J Pharm Pharmacol.* 2007;59:179–192.

27. Benevides JM, Overman SA, Thomas GJ. Raman, polarized Raman and ultraviolet resonance Raman spectroscopy of nucleic acids and their complexes. *J Raman Spectrosc.* 2005;36:279–299.

28. Lambert PJ, Whitman AG, Dyson OF, Akula SM. Raman spectroscopy: the gateway into tomorrow's virology. *Virol J.* 2006;3:51.

29. Ling J. Raman imaging microscopy—a potential cost-effective tool for drug development. *Am Pharm Rev.* 2005;8:44–49.

30. Hartschuh A, Sanchez EJ, Xie XS, Novotny L. High-resolution near-field Raman microscopy of single-walled carbon nanotubes. *Phys Rev Lett.* 2003;90:095503.

31. Li L. AbuBaker O, Shao ZJ. Characterization of poly(ethylene oxide) as a drug carrier in hot-melt extrusion. *Drug Dev Ind Pharm.* 2006;32:991–1002.

32. Bell SEJD, Andrew C, Fido LA, et al. Characterization of silicone elastomer vaginal rings containing HIV microbicide TMC120 by Raman spectroscopy. *J Pharm Pharmacol.* 2007;59:203–207.

33. Randall CS, Dinenno BK, Schultz RK, Dayter L, Konieczny M, Wunder SL. Solid-state transformation of a leukotriene antagonist. *Int J Pharm.* 1995;120:235–245.

34. Chan KLA, Fleming OS, Kazarian SG, Vassou D, Chryssikos GD, Gionis V. Polymorphism and devitrification of nifedipine under controlled humidity: a combined FT-Raman, IR and Raman microscopic investigation. *J Raman Spectrosc.* 2004;35:353–359.

35. Cao X, Sun C, Thamann TJ. A study of sulfamerazine single crystals using atomic force microscopy, transmission light microscopy, and Raman spectroscopy. *J Pharm Sci.* 2005;94:1881–1892.

36. Stoica C, Verwer P, Meekes H, Vlieg E, van Hoof PJCM, Kaspersen FM. Epitaxial 2D nucleation of the stable polymorphic form of the steroid 7αMNa on the metastable form: implications for Ostwald's rule of stages. *Int J Pharm.* 2006;309:16–24.

37. Kojima T, Onoue S, Murase N, Katoh F, Mano T, Matsuda Y. Crystalline form information from multiwell plate salt screening by use of Raman microscopy. *Pharm Res.* 2006;23:806–812.

38. Sasic S. Raman mapping of low-content API pharmaceutical formulations, I: mapping of alprazolam in alprazolam/Xanax tablets. *Pharm Res.* 2007;24:58–65.

39. Henson MJ, Zhang L. Drug characterization in low dosage pharmaceutical tablets using Raman microscopic mapping. *Appl Spectrosc.* 2006;60:1247–1255.

40. Ling J, Weitman SD, Miller MA, Moore RV, Bovik AC. Direct Raman imaging techniques for study of the subcellular distribution of a drug. *Appl Opt.* 2002;41:6006–6017.

41. Kang E, Wang H, Kwon IK, Robinson J, Park K, Cheng J-X. In situ visualization of paclitaxel distribution and release by coherent anti-stokes Raman scattering microscopy. *Anal Chem.* 2006;78:8036–8043.

42. Sasic S, Clark DA, Mitchell JC, Snowden MJ. Raman line mapping as a fast method for analyzing pharmaceutical bead formulations. *Analyst.* 2005;130:1530–1536.

43. Tian F, Sandler N, Gordon KC, et al. Visualizing the conversion of carbamazepine in aqueous suspension with and without the presence of excipients: a single crystal study using SEM and Raman microscopy. *Eur J Pharm Biopharm.* 2006;64:326–335.

44. Choo-Smith LP, Edwards HG, Endtz HP, et al. Medical applications of Raman spectroscopy: from proof of principle to clinical implementation. *Biopolymers.* 2002;67:1–9.

45. Notingher I, Hench LL. Raman microspectroscopy: a noninvasive tool for studies of individual living cells in vitro. *Expert Rev Med Devices.* 2006;3:215–234.

46. Cheng J-X, Jia K, Eheng G, Xie XS. Laser-scanning coherent anti-Stokes Raman scattering microscopy and application to cell biology. *Biophys J.* 2002;83:502–509.

47. Taleb A, Diamond J, McGarvey JJ, Beattie JR, Toland C, Hamilton PW. Raman microscopy for the chemometric analysis of tumor cells. *J Phys Chem B.* 2006;110:19625–19631.

48. de Lange MJL, Bonn M, Müller M. Direct measurement of phase coexistence in DPPC/cholesterol vesicles using Raman spectroscopy. *Chem Phys Lipids.* 2007;146:76–84.

49. Schaeberle MD, Morris HR, Turner JF, Treado PJ. Raman chemical imaging spectroscopy. *Anal Chem.* 1999;71:175A–181A.

50. Bakker Schut TC, Witjes MJH, Sterenborg HJCM, et al. In vivo detection of dysplastic tissue by Raman spectroscopy. *Anal Chem.* 2000;72:6010–6018.

51. Chowdary MVP, Kumar KK, Kurien J, Mathew S, Krishna CM. Discrimination of normal, benign, and malignant breast tissues by Raman spectroscopy. *Biopolymers.* 2006;83:556–569.

52. Yu C, Gestl E, Eckert K, Allara D, Irudayaraj J. Characterization of human breast epithelial cells by confocal Raman microspectroscopy. *Cancer Detect Prev.* 2006;30:515–522.

53. Haka AS, Shafer-Peltier KE, Fitzmaurice M, Crowe J, Dasari RR, Feld MS. Diagnosing breast cancer by using Raman spectroscopy. *Proc Natl Acad Sci USA.* 2005;102:12371–12376.

54. Krishna CM, Kegelaerl G, Rubin S, Kartha VB, Manfait M, Sockalingum GD. Combined Fourier transform infrared and Raman spectroscopic identification approach for identification of multidrug resistance phenotype in cancer cell lines. *Biopolymers.* 2006;82:462–470.

55. Brenan CJH, Hunter IW. Confocal image properties of a confocal scanning laser visible-light FT-Raman microscope. *Appl Spectrosc.* 1995;49:971–976.

56. Breitenbach J, Schrof W, Neumann J. Confocal Raman-spectroscopy: analytical approach to solid dispersions and mapping of drugs. *Pharm Res.* 1999;16:1109–1113.

57. Noda K, Sato H, Watanabe S, Yokoyama S, Tashiro H. Efficient characterization for protein crystals using confocal Raman spectroscopy. *Appl Spectrosc.* 2007;61:11–18.

58. Caspers PJ, Williams AC, Carter EA, et al. Monitoring the penetration enhancer dimethyl sulfoxide in human stratum corneum in vivo by confocal Raman spectroscopy. *Pharm Res.* 2002;19: 1577–1580.

59. Zhang G, Moore DJ, Sloan KB, Flach CR, Mendelsohn R. Imaging the prodrug-to-drug transformation of a 5-fluorouracil derivative in skin by confocal Raman microscopy. *J Invest Dermatol.* 2007;127:1205–1209.

60. Xiao C, Moore DJ, Rerek ME, Flach CR, Mendelsohn R. Feasibility of tracking phospholipid permeation into skin using infrared and Raman microscopic imaging. *J Invest Dermatol.* 2005;124:622–632.

61. Caspers PJ, Lucassen GW, Puppels GJ. Combined in vivo confocal Raman spectroscopy and confocal microscopy of human skin. *Biophys J.* 2003;85:572–580.

62. Xie C, Mace J, Dinno MA, et al. Identification of single bacterial cells in aqueous solution using confocal laser tweezers Raman spectroscopy. *Anal Chem.* 2005;77:4390–4397.

63. Chan JW, Esposito AP, Talley CE, Hollars CW, Lane SM, Huser T. Reagentless identification of single bacterial spores in aqueous solution by confocal laser tweezers Raman spectroscopy. *Anal Chem.* 2004;76:599–603.

64. Xie CG, Chen D, Li YQ. Raman sorting and identification of single living micro-organisms with optical tweezers. *Opt Lett.* 2005;30:1800–1802.

65. Chan JW, Taylor DS, Zwerdling T, Lane SM, Ihara K, Huser T. Micro-Raman spectroscopy detects individual neoplastic and normal hematopoietic cells. *Biophys J.* 2005;90:648–656.

66. Mannie MD, McConnell TJ, Xie C, Li YQ. Activation-dependent phases of T cells distinguished by use of optical tweezers and near infrared Raman spectroscopy. *J Immunol Methods.* 2005;297:53–60.

67. Deng JL, Wei Q, Zhang MH, Wang YZ, Li YQ. Study of the effect of alcohol on single human red blood cells using near-infrared laser tweezers Raman spectroscopy. *J Raman Spectrosc.* 2005;36: 257–261.

68. Ward S, Perkins M, Zhang JX, et al. Identifying and mapping surface amorphous domains. *Pharm Res.* 2005;22:1195–1202.

69. Clarke FC, Jamieson MJ, Clark DA, Hammond SV, Jee RD, Moffat AC. Chemical image fusion. The synergy of FT-NIR and Raman mapping microscopy to enable a more complete visualization of pharmaceutical formulations. *Anal Chem.* 2001;73:2213–2220.

70. Ringqvist A, Taylor L, Ekelund K, Ragnarsson G, Engstrom S, Axelsson A. Atomic force microscopy analysis and confocal Raman microimaging of coated pellets. *Int J Pharm.* 2003;267:35–47.

71. Vo-Dinh T, Yan F, Wabuyele MB. Surface-enhanced Raman scattering for medical diagnostics and biological imaging. *J Raman Spectrosc.* 2005;36:640–647.

72. Howes BD, Scatragli S, Marzocchi MP, Smulevich G. Surface-enhanced resonance Raman spectroscopy of rifamycins on silver nanoparticles: insight into their adsorption mechanisms. *J Raman Spectrosc.* 2006;37:900–909.

73. Farquharson S, Shende C, Inscore FE, Maksymiuk P, Gift A. Analysis of 5-fluorouracil in saliva using surface-enhanced Raman spectroscopy. *J Raman Spectrosc.* 2005;36:208–212.

74. Rivas L, Sanchez-Cortes S, Garcia-Ramos JV. Raman structural study of thymine and its 2 '-deoxy-ribosyl derivatives in solid state, aqueous solution and when adsorbed on silver nanoparticles. *Phys Chem Chem Phys.* 2002;4:1943–1948.

75. Rivas L, Sanchez-Cortes S, Garcia-Ramos JV. Conformational study of AZT in aqueous solution and adsorbed on a silver surface by means of Raman spectroscopy. *J Raman Spectrosc.* 2002;33:6–9.

76. Wang Y, Li YS, Wu J, Zhang ZX, An DQ. Surface-enhanced Raman spectra of some anti-tubercle bacillus drugs. *Spectrochim Acta [A].* 2000;56:2637–2644.

77. Fabriciova G, Sanchez-Cortes S, Garcia-Ramos JV, Miskovsky P. Joint application of micro-Raman and surface-enhanced Raman spectroscopy to the interaction study of the antitumoral anthraquinone drugs danthron and quinizarin with albumins. *J Raman Spectrosc.* 2004;35:384–389.

78. Lee S, Kim S, Choo J, et al. Biological imaging of HEK293 cells expressing PLC1 using surface-enhanced Raman microscopy. *Anal Chem.* 2007;79:916–922.

79. Eliasson C, Engelbrektsson J, Loren A, Abrahamsson J, Abrahamsson K, Josefson M. Multivariate methodology for surface enhanced Raman chemical imaging of lymphocytes. *Chemometr Intell Lab Sys.* 2006;81:13–20.

80. Nithipatikom K, McCoy MJ, Hawi SR, Nakamoto K, Adar F, Campbell WB. Characterization and application of Raman labels for confocal Raman microspectroscopic detection of cellular proteins in single cells. *Anal Biochem.* 2003;322:198–207.

81. Strehle KR, Cialla D, Rosch P, Henkel T, Kohler M, Popp J. A reproducible surface-enhanced Raman spectroscopy approach. Online SERS measurements in a segmented microfluidic system. *Anal Chem.* 2007;79:1542–1547.

82. Jarvis RM, Brooker A, Goodacre R. Surface-enhanced Raman spectroscopy for bacterial discrimination utilizing a scanning electron microscope with a Raman spectroscopy interface. *Anal Chem.* 2004;76:5198–5202.

83. Driskell JD, Kwarta KM, Lipert RJ, Porter MD, Neill JD, Ridpath JF. Low-level detection of viral pathogens by a surface-enhanced Raman scattering based immunoassay. *Anal Chem.* 2005;77:6147–6154.

84. Deckert V, Zeisel D, Zenobi R, Vo-Dinh T. Near-field surface-enhanced Raman imaging of dye-labeled DNA with 100-nm resolution. *Anal Chem.* 1998;70:2646–2650.

85. Rasmussen A, Deckert V. Surface- and tip-enhanced Raman scattering of DNA components. *J Raman Spectrosc.* 2006;37: 311–317.

86. Schweiger G. Raman scattering on single aerosol particles and on flowing aerosols: a review. *J Aerosol Sci.* 1990;21:483–509.

87. Reid JP, Meresman H, Mitchem L, Symes R. Spectroscopic studies of the size and composition of single aerosol droplets. *Int Rev Phys Chem.* 2007;26:139–192.

88. Rosen H, Novakov T. Raman-scattering and characterization of atmospheric aerosol particles. *Nature.* 1977;266:708–710.

89. Buehler MF, Allen TM, Davis EJ. Microparticle Raman spectroscopy of multicomponent aerosols. *J Colloid Interface Sci.* 1991;146:79–89.

90. Stowers M, Friedlander S. Chemical characterization of flowing polydisperse aerosols by Raman spectroscopy. *Aerosol Sci Technol.* 2002;36:48–61.

91. Vehring R, Aardahl C, Schweiger G, Davis E. The characterization of fine particles originating from an uncharged aerosol: size dependence and detection limits for Raman analysis. *J Aerosol Sci.* 1998;29:1045–1061.

92. Nelson MP, Zugates CT, Treado PJ, Casuccio GS, Exline DL, Schlaegle SF. Combining Raman chemical imaging and scanning electron microscopy to characterize ambient fine particulate matter. *Aerosol Sci Technol.* 2001;34:108–117.

93. Batonneau Y, Sobanska S, Laureyns J, Bremard C. Confocal microprobe Raman imaging of urban tropospheric aerosol particles. *Environ Sci Technol.* 2006;40:1300–1306.

94. Hopkins RJ, Reid JP. A comparative study of the mass and heat transfer dynamics of evaporating ethanol/water, methanol/water, and 1-propanol/water aerosol droplets. *J Phys Chem B.* 2006;110: 3239–3249.

95. Hopkins RJ, Reid JP. Evaporation of ethanol/water droplets: examining the temporal evolution of droplet size, composition and temperature. *J Phys Chem A.* 2005;109:7923–7931.

96. Mitchem L, Hopkins RJ, Buajarern J, Ward AD, Reid JP. Comparative measurements of aerosol droplet growth. *Chem Phys Lett.* 2006;432:362–366.

97. Mitchem L, Buajarern J, Hopkins RJ, et al. Spectroscopy of growing and evaporating water droplets: exploring the variation in equilibrium droplet size with relative humidity. *J Phys Chem A.* 2006;110:8116–8125.

98. Reid JP, Mitchem L. Laser probing of single-aerosol droplet dynamics. *Annu Rev Phys Chem.* 2006;57:245–271.

99. Buehler MF, Davis EJ. A study of gas aerosol chemical reactions by microdroplet Raman spectroscopy—the bromine/1-octadecene reaction. *Colloids Surf A.* 1993;79:137–149.

100. Rassat SD, Davis EJ. Chemical reaction of sulfur dioxide with a calcium oxide aerosol particle. *J Aerosol Sci.* 1992;23:165–180.

101. Chen B, Laucks M, Davis E. Carbon dioxide uptake by hydrated lime aerosol particles. *Aerosol Sci Technol.* 2004;38:588–597.

102. Tang IN, Fung KH. Characterization of inorganic salt particles by Raman spectroscopy. *J Aerosol Sci.* 1989;20:609–617.

103. Davis EJ, Rassat SD, Foss W. Measurement of aerosol/gas reaction rates by microparticle Raman spectroscopy. *J Aerosol Sci.* 1992;23:429–432.

104. Davis EJ, Aardahl CL, Widmann JF. Raman studies of aerosol chemical reactions. *J Dispersion Sci Technol.* 1998;19:293–309.

105. Zhang JX, Aiello D, Aker PM. Hydrogen-bonding at the aerosol interface. *J Phys Chem A.* 1995;99:721–730.

106. Fung KH, Tang IN. Aerosol particle analysis by resonance Raman spectroscopy. *J Aerosol Sci.* 1992;23:301–307.

107. Mitchem L, Buajarern J, Ward AD, Reid JP. A strategy for characterizing the mixing state of immiscible aerosol components and the formation of multiphase aerosol particles through coagulation. *J Phys Chem B.* 2006;110:13700–13703.

108. Spurny KR. On the chemical detection of bioaerosols. *J Aerosol Sci.* 1994;25:1533–1547.

109. Laucks ML, Roll G, Schweiger G, Davis EJ. Physical and chemical (Raman) characterization of bioaerosols—pollen. *J Aerosol Sci.* 2000;31:307–319.

110. Pan YL, Boutou V, Bottiger J, Zhang S, Wolf JP, Chang R. A puff of air sorts bioaerosols for pathogen identification. *Aerosol Sci Technol.* 2004;38:598–602.

111. Sengupta A, Laucks ML, Dildine N, Drapala E, Davis EJ. Bioaerosol characterization by surface-enhanced Raman spectroscopy (SERS). *J Aerosol Sci.* 2005;36:651–664.

112. Sengupta A, Brar N, Davis EJ. Bioaerosol detection and characterization by surface-enhanced Raman spectroscopy. *J Colloid Interface Sci.* 2007;309:36–43.

113. Kalasinsky KS, Hadfield T, Shea AA, et al. Raman chemical imaging spectroscopy reagentless detection and identification of pathogens: signature development and evaluation. *Anal Chem.* 2007;79:2658–2673.

114. Zhang XY, Young MA, Lyandres O, Van Duyne RP. Rapid detection of an anthrax biomarker by surface-enhanced Raman spectroscopy. *J Am Cancer Soc.* 2005;127:4484–4489.

115. Vincent J, Revak S, Cochrane C, Levin I. Raman spectroscopic studies of model human pulmonary surfactant systems: phospholipid interactions with peptide paradigms for the surfactant protein SP-B. *Biochemistry.* 1991;30:8395–8401.

116. Vincent JS, Revak SD, Cochrane CD, Levin IW. Interactions of model human pulmonary surfactants with a mixed phospholipid bilayer assembly—Raman spectroscopic studies. *Biochemistry.* 1993;32:8228–8238.

117. Hickey AJ, Mansour HM. Formulation challenges of powders for the delivery of small molecular weight molecules as aerosols. In: Rathbone MJ, Hadgraft J, Roberts MS, Lane M, eds. *Modified-Release Drug Delivery Technology.* 2nd ed. New York, NY: Informa Healthcare; In press.

118. Krafft C, Knetschke T, Funk RHW, Salzer R. Studies on stress-induced changes at the subcellular level by Raman microspectroscopic mapping. *Anal Chem.* 2006;78:4424–4429.

119. Kaminaka S, Yamazaki H, Ito T, Kohda E, Hamaguchi HO. Near-infrared Raman spectroscopy of human lung tissues: possibility of molecular-level cancer diagnosis. *J Raman Spectrosc.* 2001;32: 139–141.

120. Kaminaka S, Ito T, Yamazaki H, Kohda E, Hamaguchi H. Near-infrared multichannel Raman spectroscopy toward real-time in vivo cancer diagnosis. *J Raman Spectrosc.* 2002;33:498–502.

121. Koljenovic S, Schut TCB, van Meerbeeck JP, et al. Raman microspectroscopic mapping studies of human bronchial tissue. *J Biomed Opt.* 2004;9:1187–1197.

122. Huang Z, McWilliams A, Lam S, et al. Effect of formalin fixation on the near-infrared Raman spectroscopy of normal and cancerous human bronchial tissues. *Int J Oncol.* 2003;23:649–655.

123. Huang Z, McWilliams A, Lui H, McLean DI, Lam S, Zeng HS. Near-infrared Raman spectroscopy for optical diagnosis of lung cancer. *Int J Cancer.* 2003;107:1047–1052.

124. Min YK, Yamamoto T, Kohda E, Ito T, Hamaguchi H. 1064 nm near-infrared multichannel Raman spectroscopy of fresh human lung tissues. *J Raman Spectrosc.* 2005;36:73–76.

125. Kreher C, Bootz W, Niemann M, Scaffidi L, Spallek MW. Foreign particle characterization in inhalation drug products: a critical comparison of methods and techniques. In: Dalby RN, Byron PR, Suman JD, Peart J, Farr SJ, eds. *Respiratory Drug Delivery IX.* Palm Springs, CA: Davis Healthcare International Publishing; 2004:373–376.

126. Dem C, Egen M, Krueger M, Popp J. Understanding the spray dry design process through single droplet investigations. In: Dalby RN, Byron PR, Suman JD, Peart J, Farr SJ, eds. *Respiratory Drug Delivery X.* Boca Raton, FL: Davis Healthcare International Publishing; 2006:257–266.

127. Niemann M, Fusser M, Scaffidi L. A critical comparison: particle counting with light obscuration and automated Raman microscopy. In: Dalby RN, Byron PR, Suman JD, Peart J, Farr SJ, eds. *Respiratory*

Drug Delivery X. Boca Raton, FL: Davis Healthcare International Publishing; 2006:529–532.

128. Hickey AJ, Mansour HM, Telko MJ, et al. Physical characterization of component particles included in dry powder inhalers, I: strategy review and static characteristics. *J Pharm Sci.* 2007;96:1282–1301.

129. Hickey AJ, Mansour HM, Telko MJ, et al. Physical characterization of component particles included in dry powder inhalers, II: dynamic characteristics. *J Pharm Sci.* 2007;96:1302–1319.

130. Ticehurst MD, York P, Rowe RC, Dwivedi SK. Characterisation of the surface properties of α-lactose monohydrate with inverse gas chromatography, used to detect batch variation. *Int J Pharm.* 1996;141:93–99.

131. Murphy BM, Prescott SW, Larson I. Measurement of lactose crystallinity using Raman spectroscopy. *J Pharm Biomed Anal.* 2005;38:186–190.

132. Niemela P, Paallysaho M, Harjunen P, et al. Quantitative analysis of amorphous content of lactose using CCD-Raman spectroscopy. *J Pharm Biomed Anal.* 2005;37:907–911.

133. Kirk JH, Dann SE, Blatchford CG. Lactose: a definitive guide to polymorph determination. *Int J Pharm.* 2007;334:103–114.

134. Ticehurst MD, Rowe RC, York P. Determination of the surface properties of two batches of salbutamol sulphate by inverse gas chromatography. *Int J Pharm.* 1994;111:241–249.

135. Brown AB, York P, Williams AC, Edwards HGM, Worthington H. Solid-state characterization of salbutamol salts using FT-Raman and SSNMR spectroscopy. *J Pharm Pharmacol.* 1993;45:1135.

136. Moshashaée S, Bisrat M, Forbes RT, Quinn ÉA, Nyqvist H, York P. Supercritical fluid processing of proteins: lysozyme precipitation from aqueous solution. *J Pharm Pharmacol.* 2003;55:185–192.

137. Quinn EA, Forbes RT, Williams AC, Oliver MJ, McKenzie L, Purewal TS. A Raman spectroscopic study of the compatibility of proteins with hydrofluoroalkane propellants. In: Dalby RN, Byron PR, Suman JD, Peart J, Farr SJ, eds. *Respiratory Drug Delivery VII.* Tarpon Springs, FL: Davis Healthcare International Publishing; 2000:581–584.

138. Quinn EA, Forbes RT, Williams AC, Oliver MJ, McKenzie L, Purewal TS. Protein conformational stability in the hydrofluoroalkane propellants tetrafluoroethane and heptafluoropropane analysed by Fourier transform Raman spectroscopy. *Int J Pharm.* 1999;186: 31–41.

139. Guo C, Doub WH. Use of Raman imaging for determination of the particle size distribution (PSD) of active pharmaceutical ingredients (APIs) in metered dose inhalers. In: Dalby RN, Byron PR, Suman JD, Peart J, Farr SJ, eds. *Respiratory Drug Delivery X.* Boca Raton, FL: Davis Healthcare International Publishing; 2006:617–620.

140. Waligorski A, Doub WH, Adams WP, et al. Raman chemical imaging for drugs and excipients in aqueous suspension nasal spray formulations. In: Dalby RN, Byron PR, Suman JD, Pert J, Farr SJ, eds. *Respiratory Drug Delivery X.* 541–544.

141. Doub WH, Adams WP, Spencer JA, Buhse LF, Nelson MP, Treado PJ. Raman chemical imaging for ingredient-specific particle size characterization of aqueous suspension nasal spray formulations: a progress report. *Pharm Res.* 2007;24:934–945.

142. Vehring R. Red-excitation dispersive Raman spectroscopy is a suitable technique for solid-state analysis of respirable pharmaceutical powders. *Appl Spectrosc.* 2005;59:286–292.

143. Chan H, Clark AR, Feeley J, et al. Physical stability of salmon calcitonin spray-dried powders for inhalation. *J Pharm Sci.* 2004; 93:792–804.

144. Vehring R. Linear Raman spectroscopy on aqueous aerosols: influence of nonlinear effects on detection limits. *J Aerosol Sci.* 1998;29:65–79.

145. Steele DF, Young PM, Price R, Smith T, Edge S, Lewis D. The potential use of Raman mapping to investigate *in vitro* deposition of combination pressurized metered-dose inhalers. *AAPS J.* 2004;6:E32.

146. Hickey AJ. *Inhalation Aerosols: The Physiological Basis for Therapy.* New York, NY: Informa Healthcare; 2007.

147. Theophilus A, Moore A, Prime D, Rossomanno S, Whitcher B, Chrystyn H. Co-deposition of salmeterol and fluticasone propionate by a combination inhaler. *Int J Pharm.* 2006;313:14–22.

148. Michael Y, Snowden MJ, Chowdhry BZ, Ashurst IC, Davies-Cutting CJ, Riley T. Characterisation of the aggregation behaviour in a salmeterol and fluticasone propionate inhalation aerosol system. *Int J Pharm.* 2001;221:165–174.